British Journal of Applied Science & Technology

21(3): 1-11, 2017; Article no.BJAST.31893
ISSN: 2231-0843, NLM ID: 101664541

Computational Study of Aerodynamic Flow over NACA 4412 Airfoil

Moses Omolayo Petinrin[1*] and Vincent Adah Onoja[1]

[1]Department of Mechanical Engineering, University of Ibadan, Ibadan, Nigeria.

Authors' contributions

This work was carried out in collaboration between both authors. Both authors read and approved the final manuscript.

Article Information

DOI: 10.9734/BJAST/2017/31893
Editor(s):
(1) Xu Jianhua, Department of Geography, East China Normal University, China.
Reviewers:
(1) P. A. Murad, Morningstar Applied Physics, LLC, United States of America.
(2) Edisson Sávio de Góes Maciel, Instituto Tecnológico de Aeronáutica (ITA), Brazil.
Complete Peer review History: http://www.sciencedomain.org/review-history/19361

Original Research Article

Received 29th January 2017
Accepted 21st March 2017
Published 6th June 2017

ABSTRACT

The lift and drag coefficient plots for any airfoil provides a means for measuring its aerodynamic characteristics. These are very useful in deciding if a particular airfoil is appropriate for any particular application area. This study computationally predicts how the lift coefficient, drag coefficient and drag polar derived for the aerodynamic flow over the NACA 4412 airfoil vary with angles of attack. The effect of varying Reynolds number on the aerodynamic characteristics was also investigated. The finite-volume based computational fluid dynamics code; ANSYS Fluent was used to solve the continuity equation, the Reynolds Averaged Navier-Stokes equation and the turbulence transport equations governing the flow. For the range of Reynolds number considered, flow was taken as incompressible, steady and two-dimensional. Simulations were run for angles of attack ranging from -10° to 18° with an interval of 2° and for a Reynolds number range of 1.0 x 10^6 to 13.0 x 10^6. Results at a given Reynolds number revealed a steady variation between lift coefficient and angle of attack within the pre-stall region and a gradually increasing curve for the drag coefficients. A constant stalling angle at 14° with gradually increasing value for the maximum lift coefficient was recorded as the Reynolds number increased. The drag polar was also found to be constant at 6° for all the ranges of Reynolds number. The results obtained showed that numerically solving for flow problems is a valid approach for obtaining the aerodynamic characteristics of an airfoil since the results were compared with data from wind tunnel tests.

**Corresponding author: E-mail: layopet01@yahoo.com, mo.petinrin@ui.edu.ng;*

Keywords: Lift; drag; angle of attack; stall; turbulence.

1. INTRODUCTION

Aerodynamics deals with the study of the resulting effects of the relative motion between air molecules and body surfaces [1]. The impact of these interactions is quite ubiquitous: from the bending of trees as a result of wind movements, to the drag force on speeding vehicles. These responses are due to forces generated whenever there is relative motion between air molecules and body surfaces. In the field of aerodynamics, the forces mostly encountered are those of lift and Drag [2] and a special shape known as an airfoil generates these forces most efficiently [3]. The cross section of a typical airplane wing is an airfoil and is largely responsible for producing the forces that sustain the aircraft in flight [4,5].

The characteristics of any particular airfoil maybe represented by plots showing the amount of lift and drag obtained at various angles of attack as well as the drag polar [6]. By using non-dimensional coefficients, the flow over a full-scale airplane wing can be compared with the results obtained from simulating flows over model wings in a wind tunnel [7]. In the study conducted by Parashar [8] in obtaining the lift and drag curve for flow over NACA 2415, 23012 and 23015 with angles of attack ranging from -15° to +15°. It was discovered that the shapes of the airfoils have pronounced effect on their aerodynamic characteristics as they behaved differently in the same flow fields. According to Al-kayiem et al. [9], during ground collision the aerodynamic characteristics of the aircraft wing changes so much that the flow field structure around the flying body is disturbed due to the interference with the ground. They studied the aerodynamic behaviour of a NACA 4412 airfoil underground collision for a range of Reynolds number from 1.0×10^5 to 4.0×10^5 and angles of attack from -4° to 20°. It was found out that the aerodynamic characteristics were strongly influenced at angles of attack of 4° to 8°. Improvement of an aircraft performance is hinged on improving the lift produced and minimizing drag generated at the wings. This can be obtained through trailing edge optimization, control of the shock boundary layer interaction and of boundary layer separation [10] and the use of vortex generator [11,12]. A study conducted by [13] on the motion of spherical balls showed that ball dimples had better aerodynamic efficiency with increase in the overall lift and reduction in drag than the one without dimples. In the study conducted by [12] on the aerodynamic effect of the textured surface with dimples on the upper part of an aircraft wing formed from modified NACA0018 airfoil, they found out that the textured surface exhibited higher lift coefficient with drag reduction than the plain surface wing.

Experiments are carried out in wind tunnels where the flow situations are modelled after actual flight conditions and by dimensional analysis, reliable results can be obtained. However, since the advent of computational fluid dynamics (CFD) as a method of numerically obtaining the solutions to fluid flow problems, the design cycles have been shortened [6] while the huge costs of experimentations have been reduced [14]. In addition, the computer simulations show features and details that are difficult, expensive or impossible to measure or visualize experimentally [15]. Most CFD codes have different turbulent models from which the appropriate model can be chosen, depending on the kind of flow being considered. A really important aspect of a turbulence model for aerodynamic applications is its ability to accurately predict adverse pressure gradient boundary layer flows. It is especially important that a model is able to predict the location of flow separation and the wake behaviour associated with it [16].

Ravi et al. [15] predicted numerically a transition model of an incompressible laminar to turbulent flow over NACA 4412 airfoil at Reynolds number of 3.0×10^6. The lift and drag coefficients obtained from this study, using the Spalart-Allmaras and Shear Stress Transport (SST) turbulence models with transition capabilities, were compared with experimental data and concluded that the SST turbulent model had better results in both the pre-stall and post-stall region on the computational model. Eleni et al. [14] also carried out studies on the variation of lift and drag coefficients from flow around NACA 0012 airfoil at Reynolds number of 3.0×10^6 for different viscous turbulence models such as the Spalart-Allmaras, the realizable k-ε and the SST models. They concluded that SST had better agreement with experimental data. Ahmed et al. [17] utilised SST turbulence model in the study of the same airfoil but at a higher Reynolds number. The study investigated the aerodynamic characteristics of the airfoil equipped with plain

flaps (a high lift device). The behaviour of the airfoil was observed while having different flap angles at varying Mach numbers. The results showed the variation of lift coefficient with Mach number. Higher lift coefficients were obtained for higher flaps angles at any Mach number. The lift coefficient escalates with increasing Mach number but a dramatic downslope is obtained as free-stream velocity approached sonic velocity.

Although many studies have been carried out on different airfoil shapes, in this present study, the effect of varying Reynolds number on the aerodynamic characteristics of NACA 4412 will be explored at different angles of attack using the SST *k-ω* turbulence model, which has been successfully used for predicting flow over different airfoil geometries [14,15,17]. The SST model combines the advantages of the standard *k-ε* model in the free-shear flow region with that of the standard *k-ω* model in the region close to the wall. SST model is attributable to solving flow problems with adverse pressure gradient effectively [18-20].

1.1 Turbulence Modelling

Two-dimensional computational modelling of the aerodynamic characteristics of NACA 4412 airfoil was studied using the continuity equation and momentum equations. It was assumed that the flow is steady and incompressible; therefore, it was unnecessary to resolve the energy equation [17]. Thus, the governing equations are [21,22]:

i. The continuity equation

$$\frac{\partial U_j}{\partial x_j} = 0 \tag{1}$$

ii. The momentum equation

$$\rho \frac{\partial \left(U_j U_i\right)}{\partial x_j} = -\frac{\partial p}{\partial x_i} + \frac{\partial}{\partial x_j}\left[(\mu + \mu_T)\left(\frac{\partial U_i}{\partial x_j} + \frac{\partial U_j}{\partial x_i}\right) + \frac{2}{3}\rho k \delta_{ij}\right] \tag{2}$$

where x_i (i = 1, 2) represents the coordinates, U_i is the velocity vector and ρ is the density, p is the pressure, μ is the dynamic viscosity, μ_T is the turbulent eddy viscosity and k is the turbulent kinetic energy.

In order to solve for the turbulent kinetic energy, k in equation (2), the Shear Stress Transport (SST) turbulence model was employed with two additional transport equations [23]:

$$\rho \frac{\partial \left(U_j k\right)}{\partial x_j} = \tilde{P}_k - \beta^* \rho k \omega + \frac{\partial}{\partial x_j}\left[(\mu + \sigma_k \mu_T)\frac{\partial k}{\partial x_j}\right] \tag{3}$$

and

$$\rho \frac{\partial \left(U_j \omega\right)}{\partial x_j} = \gamma \rho S^2 - \beta \rho \omega^2 + \frac{\partial}{\partial x_j}\left[(\mu + \sigma_\omega \mu_T)\frac{\partial \omega}{\partial x_j}\right] + 2\left(1 - F_1\right)\rho \sigma_{w2}\frac{1}{\omega}\frac{\partial k}{\partial x_j}\frac{\partial \omega}{\partial x_j} \tag{4}$$

Where the turbulent eddy viscosity and production term, $\tilde{P}_k$ in equation (3) are given respectively as

$$\mu_T = \frac{\rho a_1 k}{\max\left(a_1 \omega, SF_2\right)} \tag{5}$$

and

$$\tilde{P}_k = \min\left[\left(\mu_T \frac{\partial U_i}{\partial x_j}\left(\frac{\partial U_i}{\partial x_j} + \frac{\partial U_j}{\partial x_i}\right)\right), 10\beta^* \rho k \omega\right] \tag{6}$$

The modulus of the mean rate-of-strain tensor, S is defined as

$$S = \sqrt{2S_{ij}S_{ij}} \tag{7}$$

here, the strain rate tensor is given as

$$S_{ij} = \frac{1}{2}\left(\frac{\partial U_i}{\partial x_j} + \frac{\partial U_j}{\partial x_i}\right) \tag{8}$$

The two blending functions, which return values between 0 and 1 are defined as

$$F_1 = \tanh\left\{\left\{\min\left[\max\left(\frac{\sqrt{k}}{\beta^* \omega y}, \frac{500\mu}{\rho y^2 \omega}\right), \frac{4\rho\sigma_{\omega 2}k}{CD_{k\omega}y^2}\right]\right\}^4\right\} \tag{9}$$

and

$$F_2 = \tanh\left[\left[\max\left(\frac{2\sqrt{k}}{\beta^* \omega y}, \frac{500\mu}{\rho y^2 \omega}\right)\right]^2\right] \tag{10}$$

From equations (9) and (10)

$$CD_{k\omega} = \max\left(2\rho\sigma_{\omega 2}\frac{1}{\omega}\frac{\partial k}{\partial x_j}\frac{\partial \omega}{\partial x_j}, 10^{-10}\right) \tag{11}$$

and y is the distance to the closest wall.

The closure constants are:

$a_1 = 0.31$ and $\beta^* = 0.09$

while the remaining closure constants are determined by blending the corresponding constants for outer surface and the inner part of the boundary layer as

$$\phi = F_1\phi_1 + (1 - F_1)\phi_2$$

Thus, the constants are computed from

$\gamma_1 = {}^5/_9$, $\gamma_2 = 0.44$, $\beta_1 = 0.075$, $\beta_2 = 0.0828$, $\sigma_{k1} = 0.85$, $\sigma_{k2} = 1.0$, $\sigma_{\omega 1} = 0.5$ and $\sigma_{\omega 2} = 0.856$.

2. COMPUTATIONAL METHODOLOGY

Two-dimensional steady aerodynamic flow over the NACA 4412 airfoil with a chord length of 1.0 m was studied numerically. Calculations were done for angles of attack ranging from -10° to 18°. The density, ρ of the air is taken as 1.225 kg/m^3 and the viscosity, μ is 1.7894×10^6 kg/ms. The Reynolds numbers considered in this study ranged from 1.0 x 10^6 to 13.0 x 10^6. Within this range, the flow can be considered as incompressible for simplicity. This is an assumption close to reality and it is not necessary to resolve the energy equation [17].

The computational domain was created using ANSYS Design Modeler while the unstructured meshes with quadrilateral elements were created in pre-processor ICEM-CFD. The resolution and density of the mesh are greater in regions where superior computational accuracy is needed, such as the near wall region of the airfoil. The generated mesh had a total of 252726 nodes and 125864 elements.

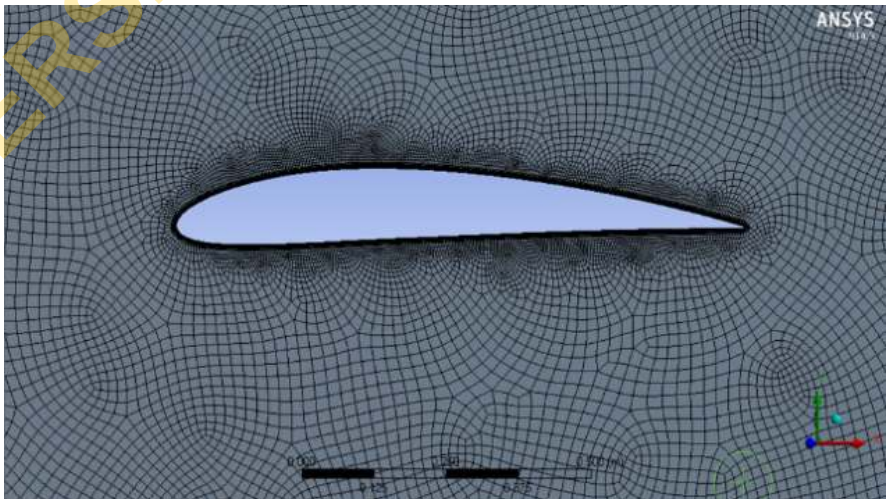

Fig. 1. Computational domain with mesh

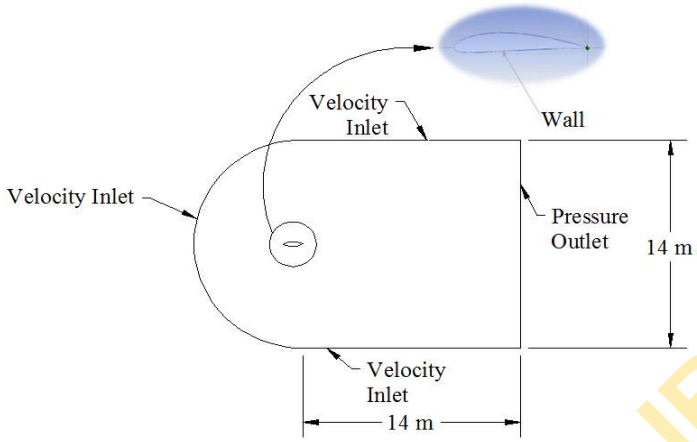

Fig. 2. Computational domain with boundary conditions

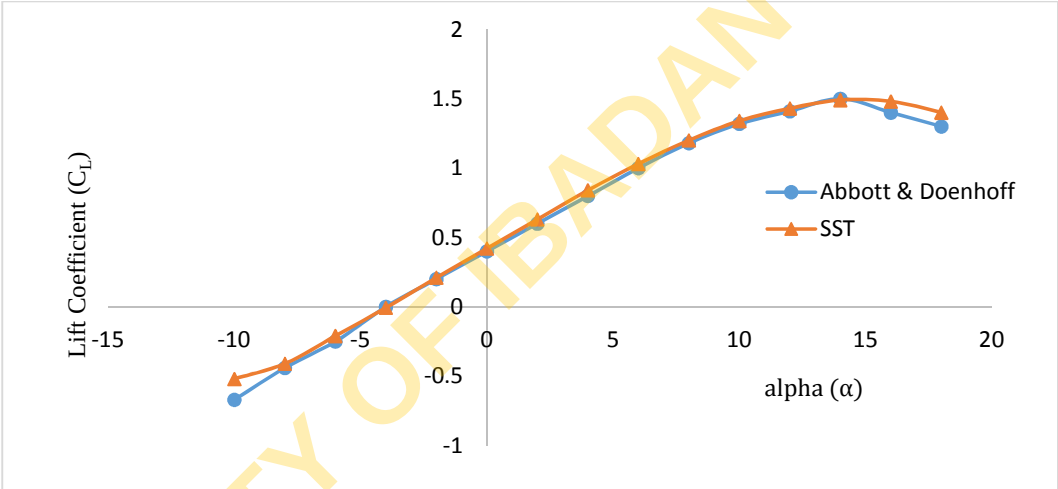

Fig. 3. Graph of lift coefficient versus angle of attack at Re = 3 x 10^6

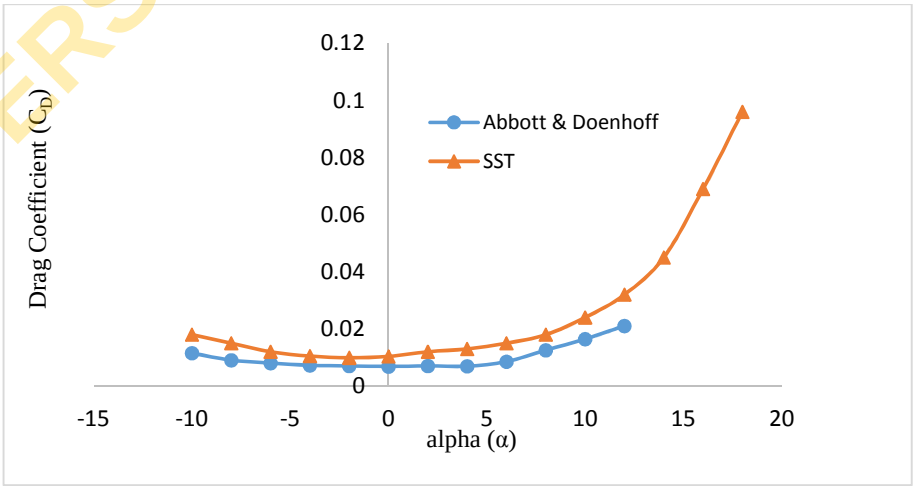

Fig. 4. Graph of drag coefficient versus angle of attack at Re = 3 x 10^6

2.1 Boundary Conditions

A finite volume based CFD code, ANSYS Fluent was used to solve the computational flow problem. The imposed boundary conditions, which include: inlet, outlet and wall boundary conditions, are as indicated in Fig. 2. The conditions set were as according to [15].

Inlet: The velocity inlet boundary condition is set which assumes the average velocity of the flow as the inlet velocity. For non-zero angles of attack, the *x* and *y* components of the velocity are given by:

$$U_x = U \cos \alpha$$
$$U_y = U \sin \alpha$$

Outlet: This is the boundary condition set at the outlet of the domain. The pressure outlet boundary condition is set, which assumes ambient atmospheric conditions.

Wall: No-slip boundary conditions are imposed. The upper and lower airfoil surfaces are treated as wall boundaries.

2.2 Validation of Simulation

Figs. 3 and 4 show the simulation results overlapped with valid experimental data from [24]. The results obtained are in close agreement with wind tunnel data, thus establishing a basis for the adoption of the computational method.

The over-prediction of drag is expected as highlighted by [14] when considering boundary layer over the airfoil as fully turbulent.

3. RESULTS AND DISCUSSION

Fig. 5 shows the variation of lift coefficient with angle of attack at a fixed Reynolds. As indicated in the figure, the lift coefficient increases steadily for angles of attack between -6° to 10°. An increase in lift coefficient is recorded with each increase angle of attack up to a maximum value recorded at 14°. Beyond this angle, a gradual decrease in the lift coefficient is observed. This angle is recognised as the stalling angle for the airfoil at the given Reynolds number. The angle of zero lift is recorded at -4° since the lift generated at this angle was zero. Negative values for lift coefficient are recorded below -4° to -10° angle of attack. This indicates the action of net downward force on the airfoil with this range of angles.

The drag characteristic of the airfoil to the one order of magnitude is as also shown in Fig. 5. The plot shows a curve decreasing gradually before reaching a minimum value at an angle of attack of -2° after which the drag coefficient continues to increase positively. Comparing the lift and drag characteristics, it is readily seen that within the positive angles of attack, lift generation is accompanied by drag generation. Also, as the stalling angle is approached, the drag coefficient rises rapidly with loss in lift.

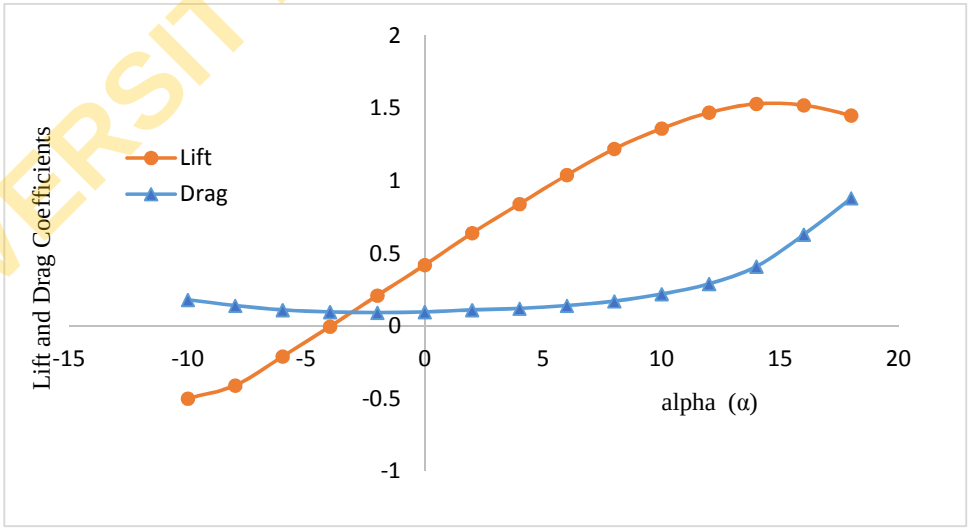

Fig. 5. Graph of lift and drag coefficient versus angle of attack at Re = 6 x 10^6

Fig. 6 shows the velocity distribution contour for the flow over the airfoil at the stall angle. It can be seen that the flow is no longer attached to the walls of the airfoil compared to the flow behaviour in Fig. 7 for angle of attack of 4°. In Fig. 7, the airfoil is at a low angle of attack, well within the region where lift coefficient is increasing with the angle of attack and the flow behaviour shows an attached flow.

The resulting drag polar is shown in Fig. 8. This plot shows the lift coefficient plotted against the drag coefficient. The maximum ratio of lift to drag coefficient was found to be at an angle of attack of 6°.

The significance of this point on the curve is that at this particular angle of attack, the airfoil optimizes lift generation by generating the least drag. If an airplane is operated in steady flight at this angle, the total drag is a minimum. At any angle of attack lower or higher, there is reduction in the lift/drag ratio and consequently increasing the total drag for a given airplane lift. This adds to fuel costs if plane is operated at this particular airspeed. Also, at the angle where lift/drag ratio is maximum, the endurance and climb angle of jet-powered airplanes is maximized [25].

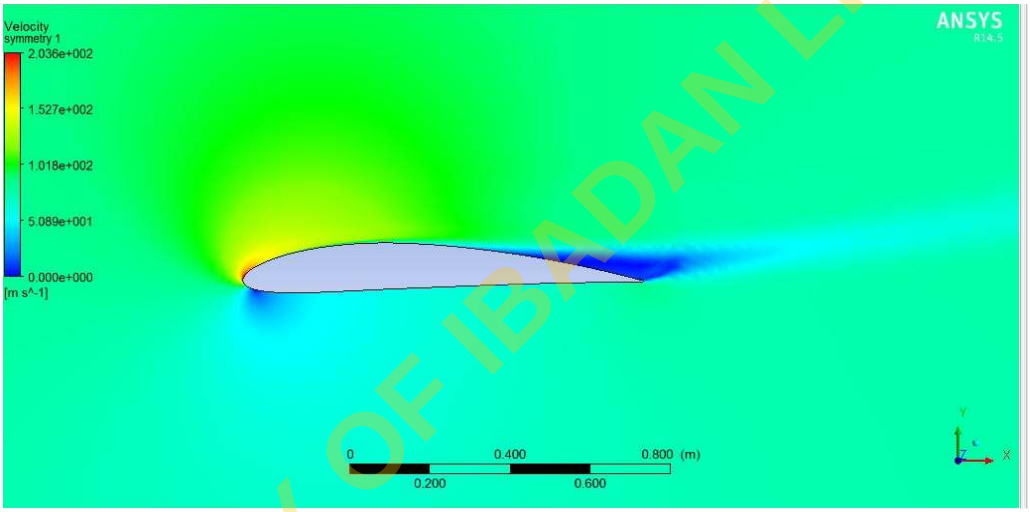

Fig. 6. Velocity distribution at stalling angle of attack (α =14°)

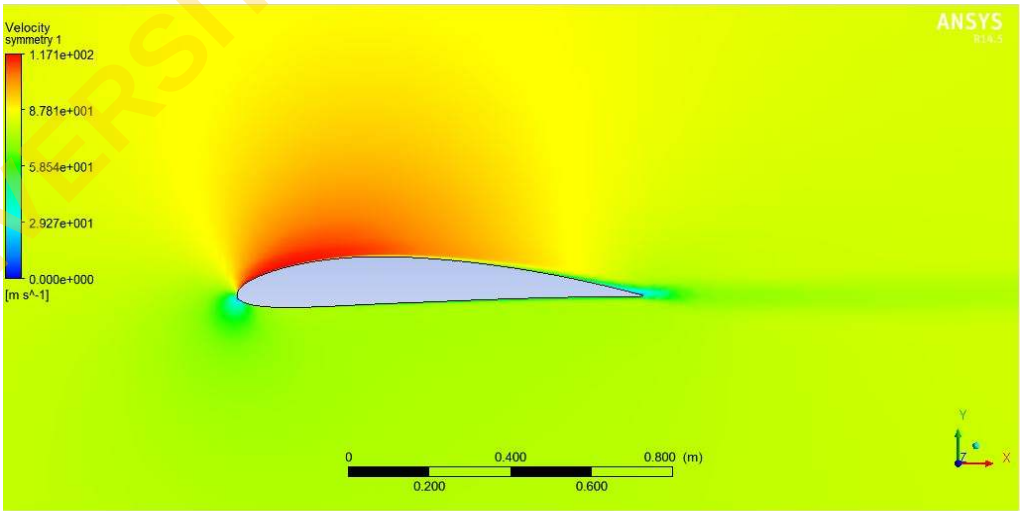

Fig. 7. Velocity distribution at 4° angle of attack

Fig. 9 shows the variation of lift coefficient with angle of attack as the Reynolds number is varied steadily. The increasing values of the lift coefficient reduce as the Reynolds number increases in the positive axis of the angle of attack. There is no or little addition to the lift as the Reynolds number increases beyond 10.0 x 10^6. The stalling angle is constant at 14°, for all the Reynolds number ranges. On the other hand Fig. 10 shows that the values for drag coefficient are lower at higher Reynolds numbers for the range of angle of attack. Also at higher Reynolds numbers, there is no much difference between the drag coefficients.

The graph plot of the drag polar against the angle of attack at different Reynolds number is as shown in Fig. 11. From this figure, the maximum drag polar is constant at 6° for all the range of Reynolds numbers considered. It is also observed that increase in drag polar reduces as the Reynolds number increases. The increment in drag polar is significantly low beyond Reynolds number of 10.0 x 10^6.

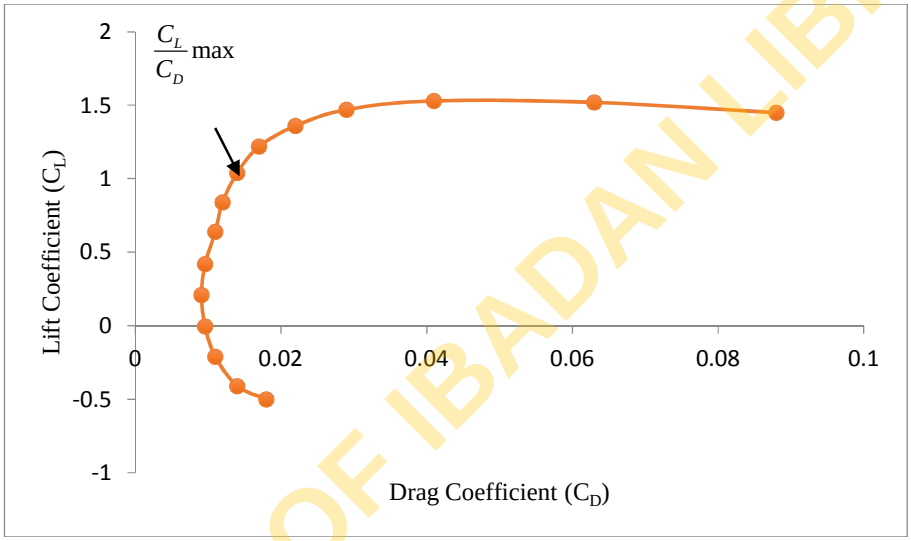

Fig. 8. The lift coefficient against drag coefficient, the Drag polar

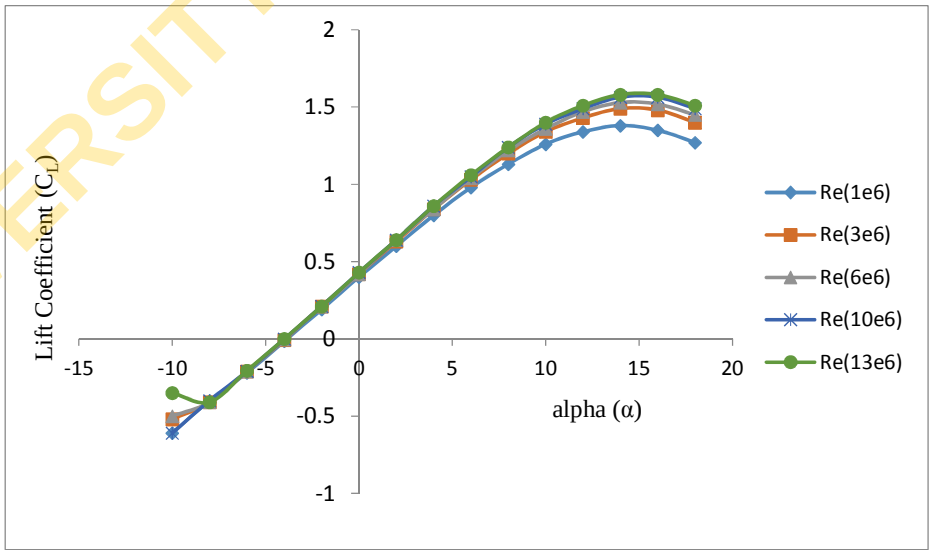

Fig. 9. The lift coefficient versus angle of attack at varying Reynolds numbers

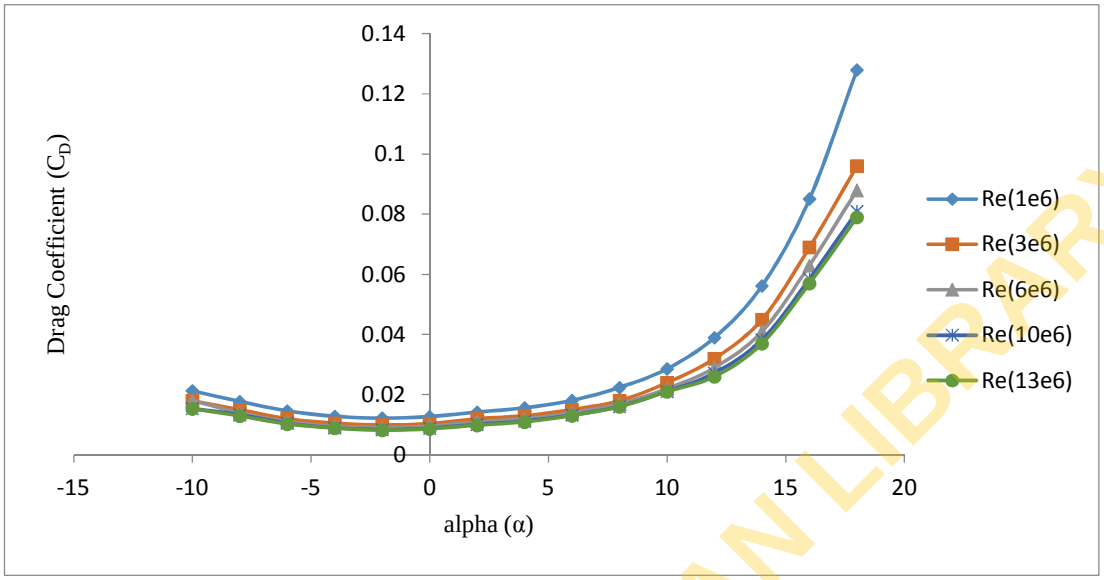

Fig. 10. The drag coefficient versus angle of attack at varying Reynolds numbers

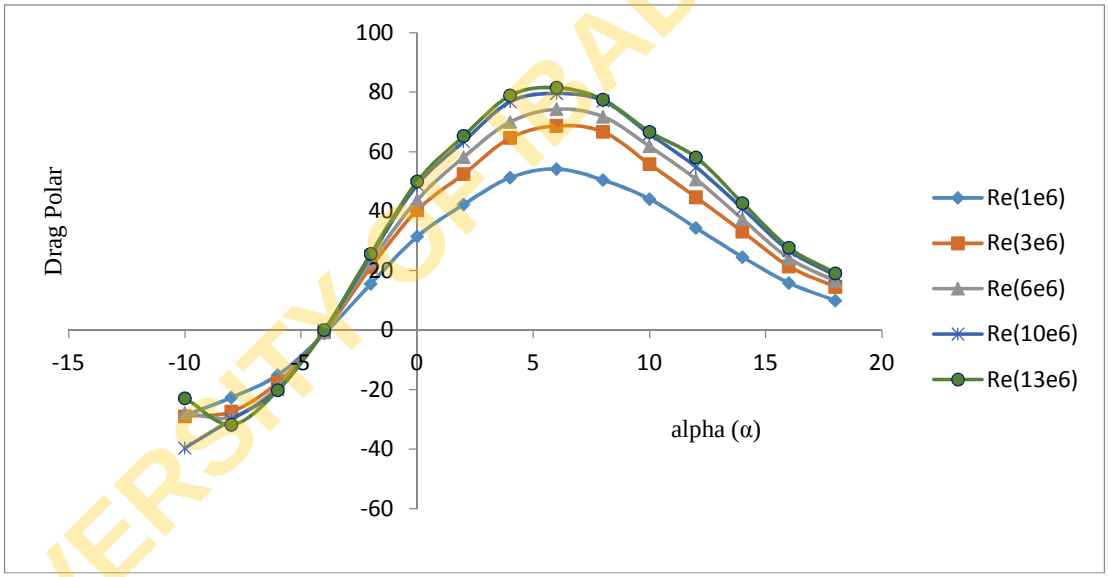

Fig. 11. The drag polar versus angle of attack at varying Reynolds numbers

4. CONCLUSION

The results obtained from this study show that numerically solving for flow problems is a valid approach for obtaining the aerodynamic characteristics of an airfoil since the results were compared with data from wind tunnel tests. The findings validate some of the theories of aerodynamics and add to the body of knowledge in the ever expanding field of airfoil design and flight control. The numerical simulation of an aerodynamic flow over NACA 4412 airfoil was studied using the SST *k-ω* transport turbulence model. The study showed that the increase in aerodynamic performance of the airfoil reduces exponentially as the Reynolds number increases.

COMPETING INTERESTS

Authors have declared that no competing interests exist.

REFERENCES

1. Fearn RL. Airfoil aerodynamics using panel methods. Math. J. 2008;10:725–739.
2. Cengel YA, Cimbala JM. Fluid mechanics: Fundamentals and applications. New York: McGraw-Hill; 2006.
3. Kevadiya M. CFD analysis of pressure coefficient for NACA 4412. International Journal of Engineering Trends and Technology. 2013;4:5.
4. Triet MM, Viet NN, Thang PM. Aerodynamic analysis of aircraft wing. VNU J. Sci. Math. – Phys. 2015;31(2):68–75.
5. Zhang Y, Fang X, Chen H, Fu S, Duan Z, Zhang Y. Supercritical natural laminar flow airfoil optimization for regional aircraft wing design. Aerosp. Sci. Technol. 2015;43: 152–164.
6. Bhosle O, Varpe R, Pula M. Radio controlled airplane. International Journal for Scientific Research & Development. 2013;3:2.
7. Darmofal D, Drela M, Uranga A. Introduction to aerodynamics. Massachusetts Institute of Technology; 2016.
(Accessed 12 December 2016)
Available:https://d37djvu3ytnwxt.cloudfront.net/assets/courseware/v1/b472b1be77ce0127b215a5c03a2736ca/asset-v1:MITx+16.101x_2+3T2015+type@asset+block/mitx_compressed.pdf
8. Parashar H. Calculation of aerodynamic characteristics of NACA 2415, 23012, 23015 airfoils using Computational Fluid Dynamics (CFD). International Journal of Science, Engineering and Technology Research. 2015;4:3.
9. Al-kayiem HH, Kartigesh AK, Chelven K. An investigation on the aerodynamic characteristics of 2-D airfoil in ground collision. Journal of Engineering Science and Technology. 2011;6(3):369-381.
10. Hiremath S, Malipatil AS. CFD simulations of aircraft body with different angle of attack and velocity. International Journal of Innovative Research in Science, Engineering and Technology. 2014;3:10.
11. Sørensen NN, Zahle F, Bak C, Vronsky T. Prediction of the effect of vortex generators on airfoil performance. J. Phys. Conf. Ser. 2014;524(1):1-11.
12. Wang XY, Lee S, Kim P, Seok J. Aerodynamic effect of 3D pattern on airfoil. Trans. Can. Soc. Mech. Eng. 2015;39(3): 537–545.
13. Srivastav D. Flow control over airfoils using different shaped dimples. International Conference on Fluid Dynamics and Thermodynamics Technologies. 2012; 33.
14. Eleni DC, Athanasios TI, Dionissios MP. Evaluation of the turbulence models for the simulation of the flow over a National Advisory Committee for Aeronautics (NACA) 0012 Airfoil. Journal of Mechanical Engineering Research. 2012;4(3):100-111.
15. Ravi HC, Madhukeshwara N, Kumarappa S. Numerical investigation of flow transition for NACA-4412 airfoil using computational fluid dynamics. International Journal of Innovative Research in Science, Engineering and Technology. 2013;2:7.
16. Badran O. Two-equation turbulence models for turbulent flow over a NACA 4412 airfoil at angle of attack 15 degree. 6th International Colloquium on Bluff Bodies Aerodynamics and Applications. 20-24 July; 2008. Milano.
17. Ahmed T, Amin T, Islam SMR, Ahmed S. Computational study of flow around a NACA 0012 wing flapped at different flap angles with varying Mach numbers. Global Journal of Researches in Engineering. 2013;13(4):4-16.
18. Menter FR. Turbulence modeling for engineering flows. *ANSYS*, Inc. 2011;1-25.
19. Rumsey C. The menter shear stress transport turbulence model; 2013. (Accessed 25 November 2015)
Available:http://turbmodels.larc.nasa.gov/sst.html
20. Woelke M. Eddy viscosity turbulence models employed by computational fluid dynamic. Transactions of the Institute of Aviation. 2007;4(191):92-113.
21. Ferziger JH, Peric M. Computational methods for fluids dynamics. 3rd ed. Berlin: Springer; 2002.
22. Wilcox DC. Turbulence modeling for CFD. 3rd ed. California: DCW; 2006.
23. Menter FR, Kuntz M, Langtry R. Ten years of industrial experience with the SST

turbulence model. Turbul. Heat Mass Transfer 4. 2003;4:625–632.

24. Abbott IH, Von-Doenhoff AE. Theory of wing sections: Including a summary of airfoil data. New York: Dover Publications, Inc; 1959.

25. Eddie S. Normals Abnormals, G450 Academics; 2014.
(Accessed 18 November 2015)
Available:http://code7700.com/l_over_d_max.html

Peer-review history:
The peer review history for this paper can be accessed here:
http://sciencedomain.org/review-history/19361